Supporting Information

Exploiting the Specific Isotope-Selective Adsorption of Metal-Organic Framework for Hydrogen Isotope Separation

Raeesh Muhammad,[†,‡] Seohyeon Jee,[§,‡], Minji Jung,[†] Jaewoo Park,[†] Sung Gu Kang,[*,¶] Kyung Min Choi,[*,§] and Hyunchul Oh[*,†,Δ]

[†]Department of Energy Engineering, Gyeongsang National University, Jinju 52725, Republic of Korea, [§]Department of Chemical and Biological Engineering, Sookmyung Women's University, 100 Cheongpa-ro 47 gil, Yongsan-gu, Seoul 04310, Republic of Korea, [¶]School of Chemical Engineering, University of Ulsan, Ulsan 44610, Republic of Korea, [Δ]Future Convergence Technology Research Institute, Jinju 52725, Republic of Korea

Experimental Details

Materials:

Cobalt (II) nitrate hexahydrate (≥98.0%), Formic acid (≥99.0%) and *N, N'*-dimethylformamide (≥99.0%) were purchased from Sigma Aldrich. Diethyl ether (99%) was purchased from Alfa Aesar.

Synthesis of Cobalt Formate, $Co_3(HCOO)_6$

Cobalt formate (CoFA) was synthesized in gram scale. Cobalt (Ⅱ) nitrate hexahydrate (17.6 mmol, 5.236 g) and Formic acid (115.7 mmol, 4.5 mL) were dissolved in *N, N'*-dimethylformamide (15 mL) using ultra sonication. The solution was heated at 100 °C overnight to synthesize crystals of Cobalt formate. The resulting purple crystals were collected and washed with DMF (10 mL) and Diethyl ether (10 mL) 3 times for each. The crystals were dried in a vacuum oven at 50° C for 5 hours. The yield of CoFA was about 93% (2.847 g).

Structural Characterizations:

The structural characterizations for CoFA have been performed by using Fourier transform infrared (FT-IR) spectroscopy, thermal gravimetric analysis (TGA) and powder X-ray diffraction (PXRD). FT-IR spectrum was recorded on a Thermo Fisher Scientific Nicolet iS50. Sample data were recorded in transmission mode in the range of 4000 to 650 cm^{-1} using ATR diamond mode with 64 scans at a resolution of 4 cm^{-1}. Thermal stability was measured using Perkin-Elmer TGA thermogravimetric analyzer in air with a heating rate 10°C/min up to 550°C. PXRD patterns of the CoFA crystals were measured using Bruker D8 Advanced (TRIO/TWIN) with scanning rate of 4°/min from 5° to 45° with a silicon holder.

Textural Characterizations and Gas Sorption Analysis:

A Highly sophisticated gas sorption analyzer autosorb-iQ2 (Quantachrome Instruments) was used to perform the textural characterizations and gas (D_2 and H_2) sorption experiments. Prior to adsorption experiments the sample cell has been calibrated for temperature, then further based on the temperature caliberation the volume caliberation of empty sample cell has been carried out. For sorption experiments, about 100 mg of sample was activated at 423 K under dynamic vacuum for 8 hrs in order to remove any adsorbed solvent or gas molecules on the sample. Textural analysis has been performed by measuring the N_2 sorption analysis at 77 K. D_2 and H_2 sorption isotherms have been measured in the temperature range of 20 to 77 K using cryo-cooler which allows us to control the temperatures from 20 K to 300 K with an estimated error of < 0.1 K.

Thermal Desorption Spectroscopic (TDS) studies for H_2 and D_2:

The thermal desorption analysis was measured by using home-built cryogenic thermal desorption spectroscopy (TDS) equipped with quadruple mass spectroscopy (QMS), and the details of it has been described previously.[S1,S2] Prior to experiment, the sample was activated at 423 K for 4 h under dynamic vacuum (10^{-8} torr). In order to quantify the signal of the mass spectrometer, TDS apparatus was calibrated by using TiH_2 and PdCe alloy. For desorption experiment with pure gas, the sample was exposed to pure H_2 and D_2 of 1 bar at 20 K and 23 K, respectively for 30 min then all the non-adsorbed gas was evacuated, after that it was cooled down to 18 K. Finally, the sample was heated at a rate of 3 K/min to 100 K. The desoprtion experiment of D_2/H_2 mixture gases was carried out using with equimolar D_2/H_2 composition at specific exposure temperature for specific exposure time. Similar to pure gases, here also all the non-adsorbed gases were evacuated before cooling down to 18 K and then subsequmet heating at a rate of 3 K/min to final temperature of 100 K while the desorbing gases were detected simultaneously by quadruple mass spectroscopy (QMS). The selectivity was obtained after quantifying the area under the desorption curve using the calibration constant.

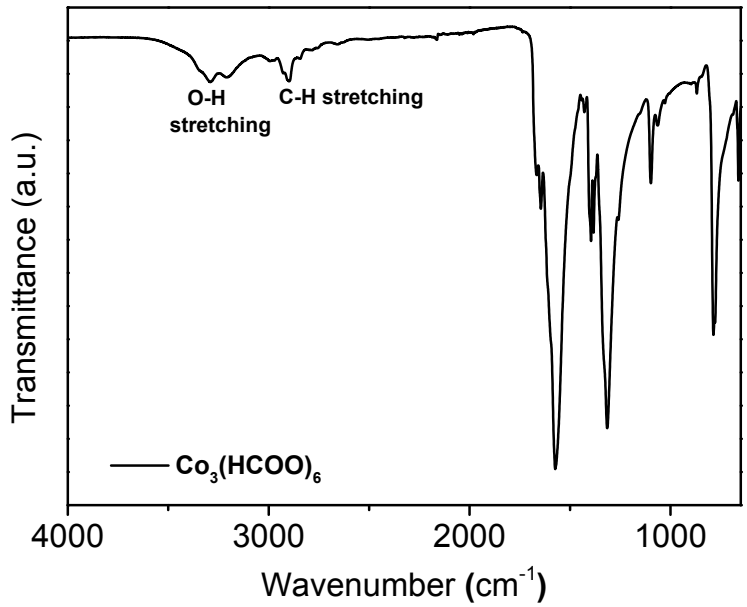

Figure S1. FT-IR spectrum of CoFA.

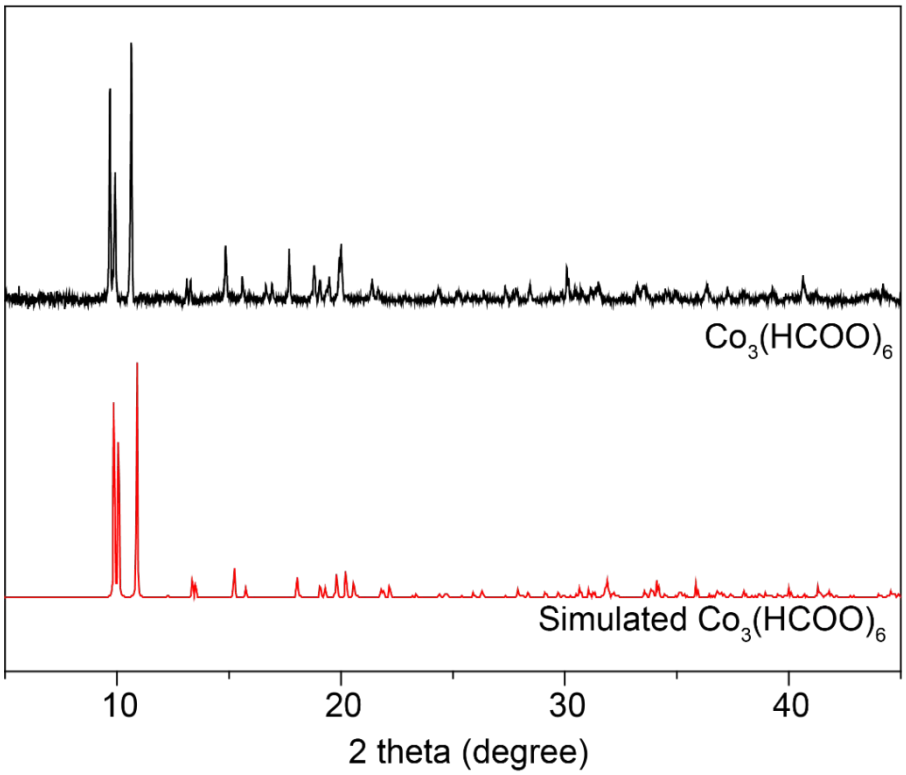

Figure S2. PXRD patterns of CoFA with the simulated PXRD patterns of desolvated CoFA.

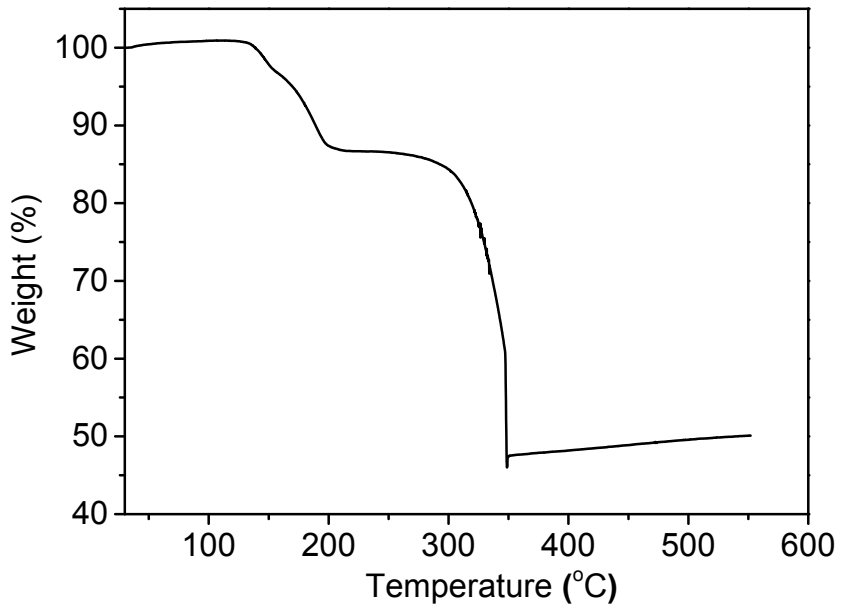

Figure S3. TGA of CoFA measured in air.

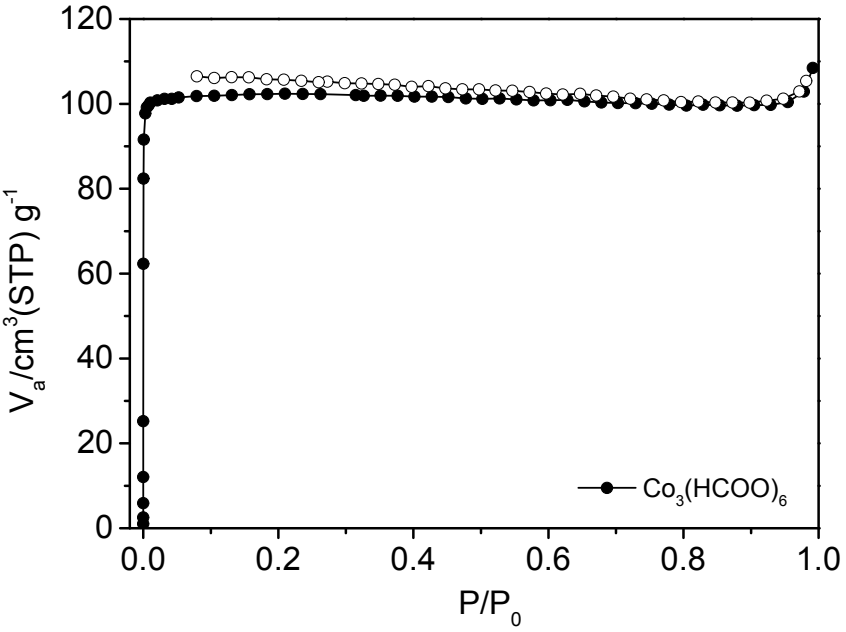

Figure S4. N_2 sorption isotherm of CoFA measured at 77 K.

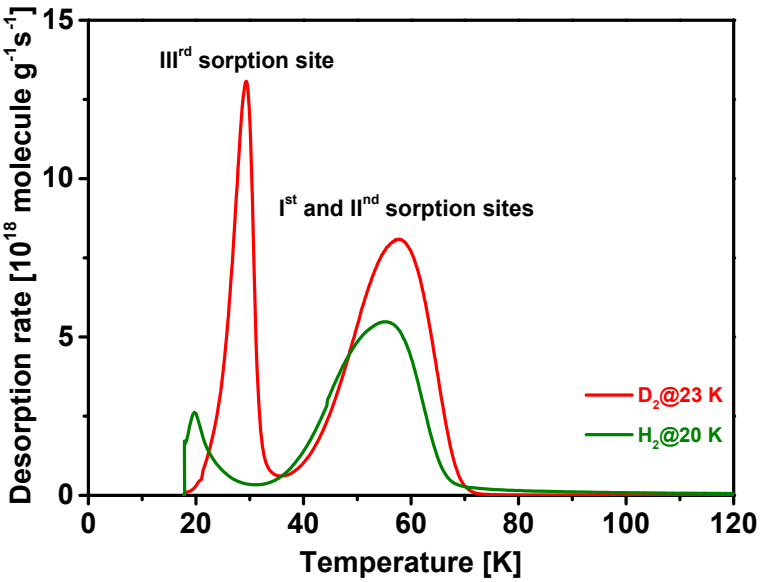

Figure S5. Pure gas (H_2 and D_2) thermal desorption spectra of CoFA measured with heating rate of 3 K min^{-1}.

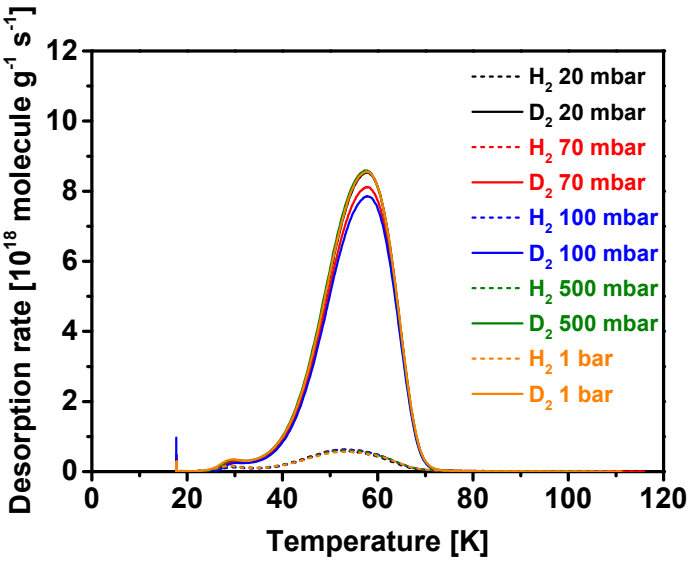

Figure S6. Equimolar D_2/H_2 mixture TDS spectra of CoFA measured at 30 K and 10 min exposure time with varying pressure loading.

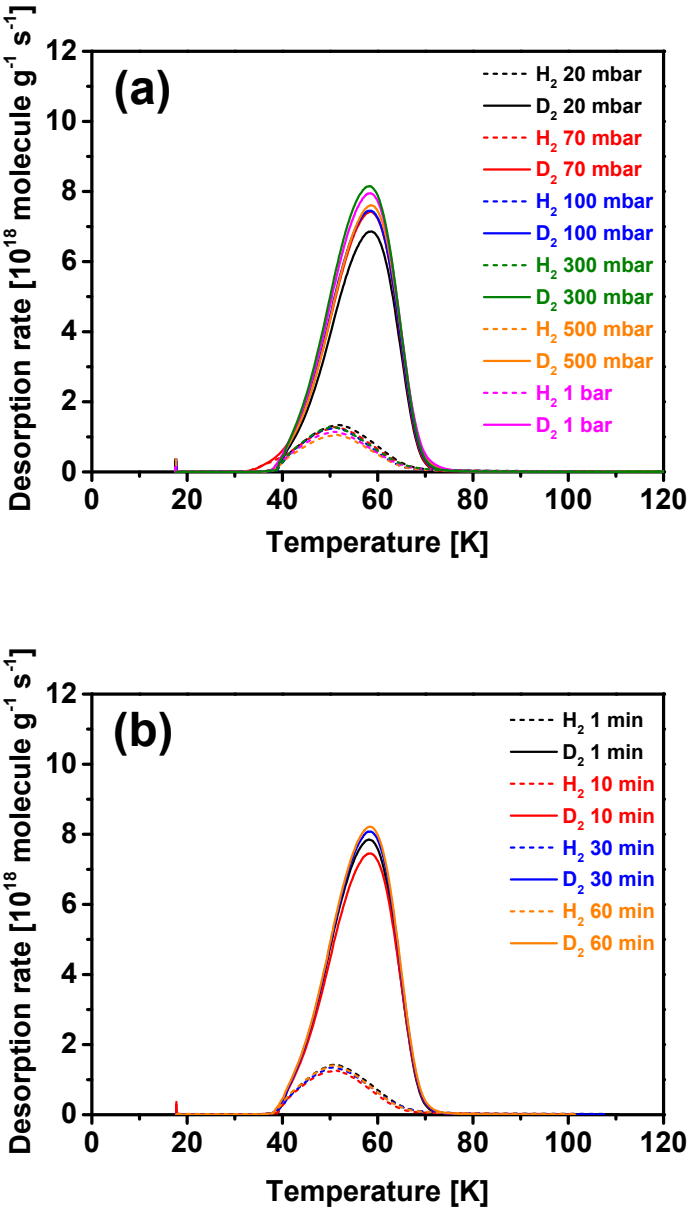

Figure S7. Equimolar D_2/H_2 mixture TDS spectra of CoFA measured at 40 K and 10 min exposure time with varying (a) pressure loading and (b) exposure time.

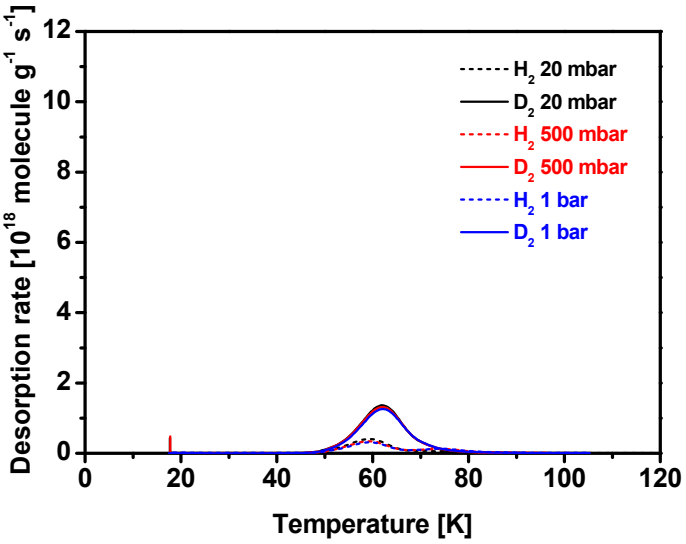

Figure S8. Equimolar D_2/H_2 mixture TDS spectra of CoFA measured at 60 K and 10 min exposure time with varying pressure loading.

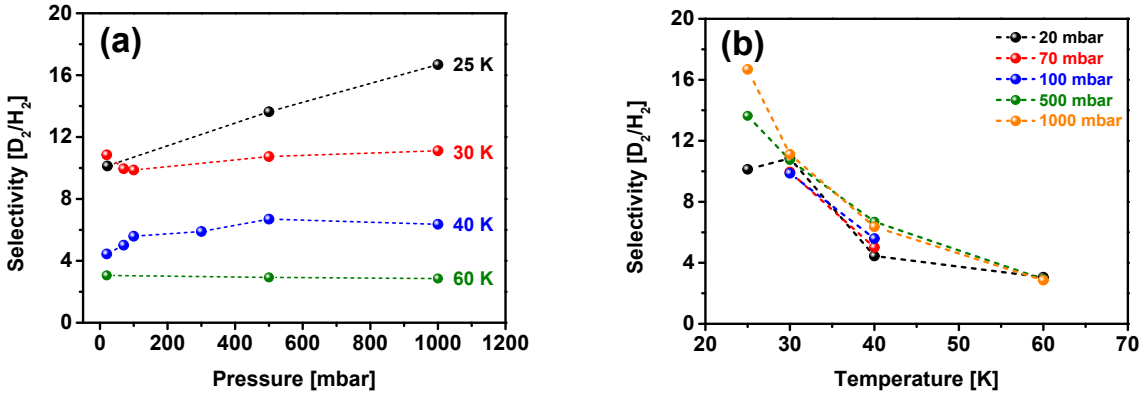

Figure S9. Equimolar D_2/H_2 mixture, $S_{D2/H2}$ as a function of (a) pressure loading and (b) exposure temperature.

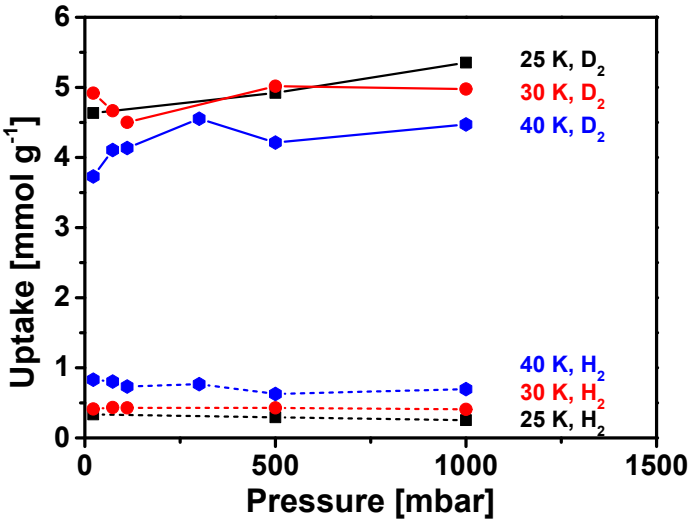

Figure S10. H_2 uptake (dotted line) and D_2 uptake (solid line) at strong binding site with increase in pressure loading at various temperatures.

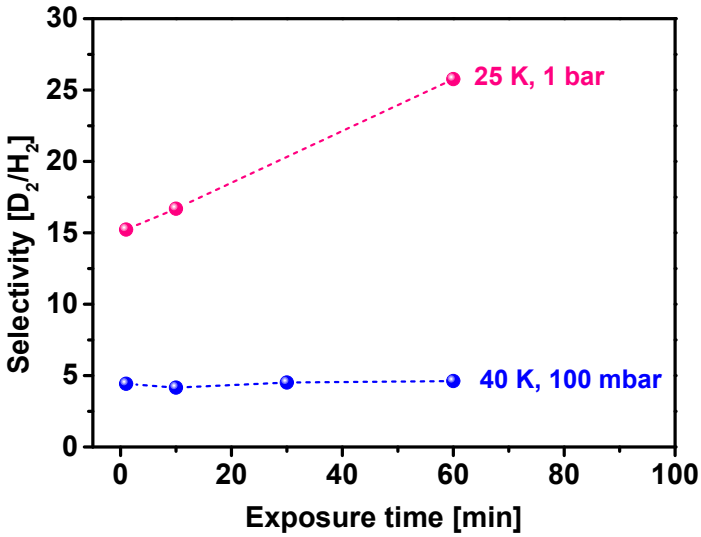

Figure S11. Equimolar D_2/H_2 mixture, $S_{D2/H2}$ as a function of exposure time at 25 K/1 bar and 40 K/100 mbar.

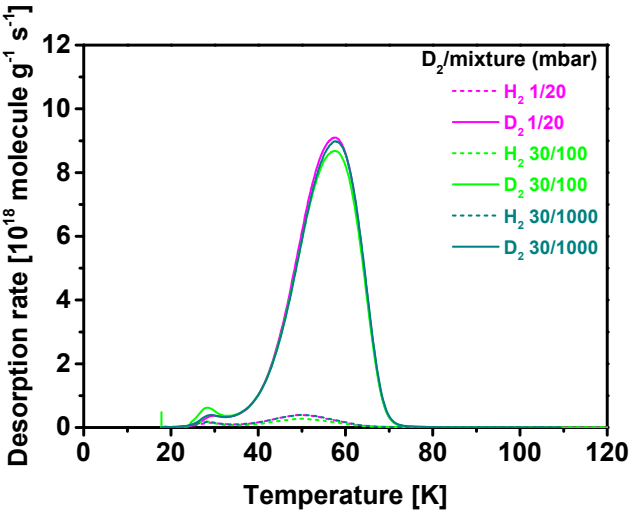

Figure S12. TDS spectra measured at 30 K and 10 min exposure time with exposure of D_2 (1 mbar to 30 mbar) and equimolar D_2/H_2 mixture (20 mbar to 1 bar).

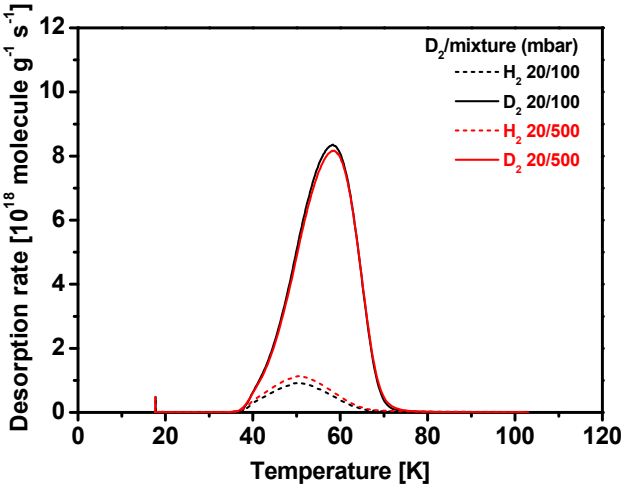

Figure S13. TDS spectra measured at 40 K and 10 min exposure time with exposure of D_2 (20 mbar) and equimolar D_2/H_2 mixture (100 and 500 mbar).

Table S1. Separation performance comparison with reported literature using 1:1 isotope mixture

Compound	Experimental Temperature (K)	D_2 uptake (mmol g^{-1})	$S_{D2/H2}$ for 1:1 isotope mixture	Reference
Cocryst1	30	4.7	8.0	S3
Zeolite 5A	30	4.0	2.7	S4
Py@COF-1	22	0.5	9.7	S1
MIL-53(Al)	40	2.9	13.6	S5
MOF-74-IM-10	77	2.8	26.0	S6
MFU-4*l*	40	8.3	1.7	S7
IFP-1	30	9.3	2.0	S8
Takeda 3A	40	0.01	6.8	S9
MFU-4(Co,Cl)	30	4.72	4	S9
MS13X	77	0.6	3.1	S10
Ni_2Cl_2BBTA	77	11	4.5	S11
Cobalt formate	**25**	**7.0**	**25.8**	**This work**

Density functional theory calculations

Vienna Ab Initio Simulation Package (VASP)[S12,S13] was employed for DFT+U calculations in this study. GGA-PBE[S14] functional was used for all calculations with the criterion of 1×10^{-4} eV (0.01 eV/Å) for energy (force) convergence. After optimizing the volume of the formate using an energy cutoff of 520 eV, the cutoff was reduced to 400 eV for later calculations. The Monkhorst–Pack *k*-meshes[S15] of $3 \times 2 \times 2$ were employed for a $1 \times 2 \times 1$ supercell. The spin polarization and the effective U value of 5.05 eV[S16] for Co were included in all calculations[S17]. Using DFT-D3 (Becke-Jonson damping) implemented in VASP, van der Waals corrections were applied to our calculations[S18-S21]. To explore the migration energies of a hydrogen/deuterium molecule in cobalt formate (CoFA), climbing image nudged elastic band (NEB)[S22] calculations were done. The binding energy (E_b) of a hydrogen molecule to CoFA was determined using eq (1) with zero-point energy corrections[S23].

$$E_b = E_{H_2/CoFA} - E_{CoFA} - E_{H_2} \quad (1)$$

where $E_{H_2/CoFA}$, E_{CoFA}, and E_{H_2} are total energies of a hydrogen molecule within the CoFA, the CoFA, and the hydrogen molecule, respectively.

As displayed in Figure S14, the classical barrier for H_2 migration inside the formate was found to be quite small as 1.09 kJ/mol. On the other hand, the binding energies of H_2 and D_2 to the formate were -5.69 and -7.95 kJ/mol, respectively, indicating that the binding strength of D_2 is higher than that of H_2 by 2.26 kJ/mol.

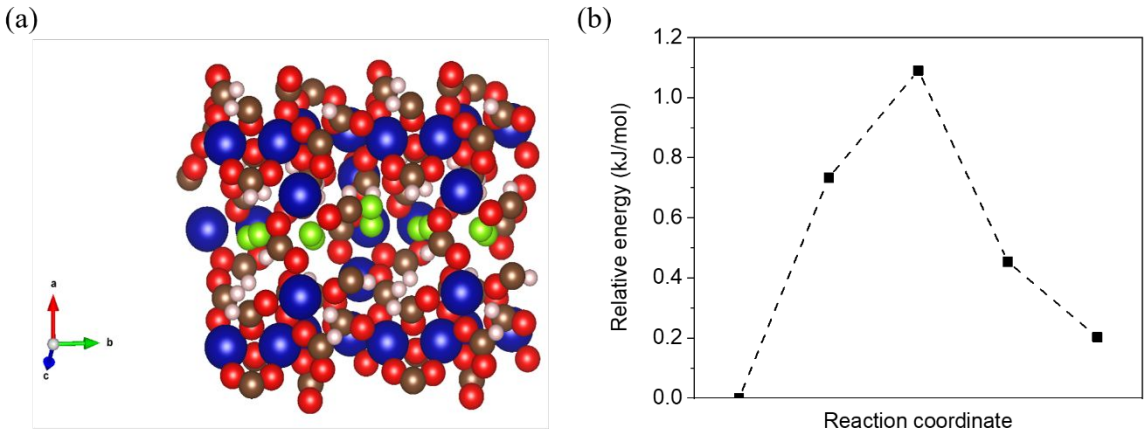

Figure S14. (a) Migration of a hydrogen molecule (H_2) inside CoFA. Blue, brown, light green, red, and white colors were employed to represent cobalt, carbon, migrated hydrogen, oxygen, and hydrogen, respectively and (b) classical energy profile for H_2 migration inside CoFA.

References

S1. Oh, H.; Kalidindi, S. B.; Um, Y.; Bureekaew, S.; Schmid, R.; Fischer, R. A.; Hirscher, M. A Cryogenically Flexible Covalent Organic Framework for Efficient Hydrogen Isotope Separation by Quantum Sieving. *Angew. Chem. Int. Ed.* **2013**, *52*, 13219–13222.

S2. Oh, H.; Savchenko, I.; Mavrandonakis, A.; Heine, T.; Hirscher, M. Highly Effective Hydrogen Isotope Separation in Nanoporous Metal–Organic Frameworks with Open Metal Sites: Direct Measurement and Theoretical Analysis. *ACS Nano* **2014**, *8*, 761–770.

S3. Liu, M;. Zhang, L.; Little, M. A.; Kapil, V.; Ceriotti, M.; Yang, S.; Ding, L.; Holden, D. L.; Balderas-Xicohténcatl, R.; He, D.; Clowes, R.; Chong, S. Y.; Schütz, G.; Chen, L.; Hirscher, M.; Cooper, A. I. Barely Porous Organic Cages for Hydrogen Isotope Separation. *Science* **2019**, *366*, 613–620.

S4. Xiong, R.; Balderas-Xicohténcatl, R.; Zhang, L.; Li, P.; Yao, Y.; Sang, G.; Chen, C.; Tang, T.; Luo, D.; Hirscher, M. Thermodynamics, Kinetics and Selectivity of H_2 and D_2 on Zeolite 5A Below 77K. *Microporous Mesoporous Mater.* **2018,** *264*, 22–27.

S5. Kim, J. Y.; Zhang, L.; Balderas-Xicohténcatl, R.; Park, J.; Hirscher, M.; Moon, H. R.; Oh, H. Selective Hydrogen Isotope Separation via Breathing Transition in MIL-53 (Al). *J. Am. Chem. Soc.* **2017**, *139*, 17743–17746.

S6. Kim, J. Y.; Balderas-Xicohténcatl, R.; Zhang, L.; Kang, S. G.; Hirscher, M.; Oh, H.; Moon, H. R. Exploiting Diffusion Barrier and Chemical Affinity of Metal–Organic Frameworks for Efficient Hydrogen Isotope Separation. *J. Am. Chem. Soc.* **2017**, *139*, 15135–15141.

S7. Savchenko, I.; Mavrandonakis, A.; Heine, T.; Oh, H.; Teufel, J.; Hirscher, M. Hydrogen Isotope Separation in Metal-Organic Frameworks: Kinetic or Chemical Affinity Quantum-Sieving? *Microporous Mesoporous Mater.* **2015,** *216*, 133–137.

S8. Mondal, S. S.; Kreuzer, A.; Behrens, K.; Schütz, G.; Holdt, H.-J.; Hirscher, M. Systematic Experimental Study on Quantum Sieving of Hydrogen Isotopes in Metal-Amide-Imidazolate Frameworks with Narrow 1-D Channels. *ChemPhysChem* **2019,** *20*, 1311–1315.

S9 Teufel, J. Experimental Investigation of H_2/D_2 Isotope Separation by Cryoadsorption in Metal-Organic Frameworks, PhD Thesis, Universität Stuttgart, Stuttgart, **2013**.

S10. Niimura, S.; Fujimori, T.; Minami, D.; Hattori, Y.; Abrams, L.; Corbin, D.; Hata, K.; Kaneko, K. Dynamic Quantum Molecular Sieving Separation of D_2 from H_2–D_2 Mixture with Nanoporous Materials. *J. Am. Chem. Soc.* **2012**, *134*, 18483-18486.

S11 Li, X.; Wang, X.; Li, M.; Luo, J.; An, Y.; Li, P.; Song, J.; Chen, C.; Feng, X.; Wang, S. Highly Selective Adsorption of D_2 from Hydrogen Isotopes Mixture in a Robust Metal Bistriazolate Framework with Open Metal Sites. *Int. J. Hydrogen Energy* **2020**, *45*, 21547-21554.

S12. Kresse, G.; Furthmüller, J. Efficient Iterative Schemes for Ab Initio Total-Energy Calculations Using a Plane-Wave Basis Set. *Phys. Rev. B* **1996,** *54*, 11169-11186.

S13. Kresse, G.; Furthmüller, J. Efficiency of Ab-Initio Total Energy Calculations for Metals and Semiconductors Using a Plane-Wave Basis Set. *Comput. Mater. Sci.* **1996**, *6*, 15-50.

S14. Perdew, J. P.; Burke, K.; Ernzerhof, M. Generalized Gradient Approximation Made Simple. *Phys. Rev. Lett.* **1996,** *77*, 3865-3868.

S15. Monkhorst, H. J.; Pack, J. D. Special Points for Brillouin-Zone Integrations. *Phys. Rev. B* **1976,** *13*, 5188-5192.

S16. Zhou, F.; Cococcioni, M.; Marianetti, C. A.; Morgan, D.; Ceder, G. First-Principles Prediction of Redox Potentials in Transition-Metal Compounds with LDA+U. *Phys. Rev. B* **2004,** *70*, 235121-235128.

S17. Dudarev, S. L.; Botton, G. A.; Savrasov, S. Y.; Humphreys, C. J.; Sutton, A. P. Electron-Energy-Loss Spectra and the Structural Stability of Nickel Oxide: An LSDA+ U Study. *Phys. Rev. B* **1998,** *57*, 1505-1509.

S18. Grimme, S.; Antony, J.; Ehrlich, S.; Krieg, H. A Consistent and Accurate Ab Initio Parametrization of Density Functional Dispersion Correction (DFT-D) for the 94 Elements H-Pu. *J. Chem. Phys*. **2010,** *132*, 154104.

S19. Grimme, S.; Ehrlich, S.; Goerigk, L. Effect of the Damping Function in Dispersion Corrected Density Functional Theory. *J. Comput. Chem.* **2011,** *32*, 1456–1465.

S20. Becke, A. D.; Johnson, E. R. A Density-Functional Model of the Dispersion Interaction. *J. Chem. Phys.* **2005,** *123*, 154101.

S21. Johnson, E. R.; Becke, A. D. A Post-Hartree-Fock Model of Intermolecular Interactions: Inclusion of Higher-Order Corrections. *J. Chem. Phys.* **2006,** *124*, 174104.

S22. Henkelman, G.; Uberuaga, B. P.; Jonsson, H. A Climbing Image Nudged Elastic Band Method for Finding Saddle Points and Minimum Energy Paths. *J. Chem. Phys.* **2000,** *113*, 9901–9904.

S23. Sholl, D. S.; Steckel, J. A. Density Functional Theory: A Practical Introduction (John Wiley & Sons, Inc., Hoboken, New Jersey, **2009**).